

Learning to Infer Unseen Attribute-Object Compositions

Hui Chen, Zhixiong Nan, Jingjing Jiang, and Nanning Zheng, *Fellow, IEEE*

Abstract—The composition recognition of unseen attribute-object is critical to make machines learn to decompose and compose complex concepts like people. Most of the existing methods are limited to the composition recognition of single-attribute-object, and can hardly distinguish the compositions with similar appearances. In this paper, a graph-based model is proposed that can flexibly recognize both single- and multi-attribute-object compositions. The model maps the visual features of images and the attribute-object category labels represented by word embedding vectors into a latent space. Then, according to the constraints of the attribute-object semantic association, distances are calculated between visual features and the corresponding label semantic features in the latent space. During the inference, the composition that is closest to the given image feature among all compositions is used as the reasoning result. In addition, we build a large-scale Multi-Attribute Dataset (MAD) with 116,099 images and 8,030 composition categories. Experiments on MAD and two other single-attribute-object benchmark datasets demonstrate the effectiveness of our approach.

Index Terms—Unseen attribute-object composition recognition, zero-shot learning, high-level vision, graph convolutional networks, multi-label learning

1 INTRODUCTION

THE ultimate goal of AI is to make machines learn and think like people. Recently, the remarkable developments [1], [2], [3] of deep learning [4] have quickened the progress toward this goal. However, machine intelligence is still far from matching human intelligence. Humans can learn richer semantic representations from fewer data and generalize in a more flexible way. Usually, only one or a few examples are needed before a human being can learn a concept that can be flexibly applied in other domains (e.g. generalizing known concepts to recognize new examples or composing multiple concepts to understand new concepts). To build a machine to learn, compose and generalize concepts like humans, this paper handles a challenging problem, which is called unseen attribute-object composition recognition. Given an image, unseen attribute-object composition recognition asks a model to simultaneously recognize the attribute type and object type of the image even though that attribute-object composition is not included in the training set. For example, the training set includes samples of “sliced tomato” and “green apple” (seen compositions), while the testing set includes samples of “sliced apple” (unseen composition). To correctly recognize unseen compositions, the model needs to learn the concepts of attributes and objects from the seen compositions and then compose and generalize the concepts to recognize unseen compositions.

Unseen attribute-object composition recognition is a meaningful problem. From the perspective of cognitive psychology, attribute is a high-level semantic description for

objects, which is closely related to the formation of abstract concepts, particularly the multi-attribute cognition of objects plays an important role in understanding the environment in people’s daily life [5]. The ability to recognize unseen compositions by inferring and generalizing assists human beings to understand new objects. Therefore, building a machine to recognize unseen attribute-object compositions like people can achieve a deeper understanding of images, allowing for advanced applications, such as image retrieval [6], pedestrian re-identification [7], scene graph generation [8], relation reasoning [9], and object perception [10], [11]. For example, compared with a system that can recognize only objects, a system that understands the concepts of attribute-object compositions can output more accurate retrieval results. In addition, recognizing unseen compositions based on those that are seen requires only data annotations of the seen compositions, relieving the resource consumption of data annotations for all compositions.

The main challenges of unseen attribute-object composition recognition are as follows: 1) Some different compositions (e.g. “scratched screen” and “broken screen”) share similar appearances in such a way that they are easily misclassified. 2) The attribute is abstract because we cannot find a proper prototype even for a simple attribute (e.g. “beautiful”). In addition, the same attribute presents diverse visual appearances in different attribute-object compositions, making it difficult to learn an intrinsic feature representation of an attribute. 3) Although there are only hundreds of attributes or objects, there could be thousands of meaningful compositions, increasing the difficulty of finding the correct composition.

Methods for unseen attribute-object composition recognition have been active throughout the transition from discriminative models to generative models. In the early times, discriminative methods typically learned attribute and object classifiers in the beginning, and then, they recognized

• H.Chen, Z. Nan, J. Jiang and N. Zheng (corresponding author) are with the Institute of Artificial Intelligence and Robotics, Xi’an Jiaotong University, Shaanxi, 710049 China (e-mail: chenhui0622@stu.xjtu.edu.cn; nzx2018@xjtu.edu.cn; jingjingjiang2017@gmail.com; nnzheng@mail.xjtu.edu.cn).

Manuscript received April 19, 2005; revised August 26, 2015.

unseen compositions by composing these separately-trained classifiers [12], [13], [14], [15]. These methods largely push forward the study of unseen attribute-object composition recognition, but separately-trained classifiers ignore the relations between the attributes and objects. Unseen attribute-object composition recognition is a high-level and complex vision problem that relies on the deep understanding of an image, which asks a model to consider the relations between the attributes and objects. Recent studies [16], [17], [18] have attempted to process the attribute and object as a whole to explore their inner relations. For example, Nagarajan et al. [17] regard an attribute as a linear transformation matrix and an object as an embedding vector, and an attribute-object composition is finally formulated as the object vector multiplied by the attribute matrix. More recently, generative models [19], [20], [21] have achieved state-of-the-art performance. For example, Nan et al. [20] learn the attribute-object relations with an encoder-decoder based generative model, which improves the recognition performance. Wei et al. [21] utilize the positive and (semi-) negative attribute-object composition embeddings to learn a more accurate correlation between the attributes and objects. Although these methods have achieved impressive progress, two problems remain to be solved: 1) How to design an effective mechanism to model the inner relations between the attributes and objects, and 2) how to distinguish the attribute-object compositions with similar appearances.

Two kinds of data modalities, visual images and the corresponding linguistic labels, are involved in unseen attribute-object composition recognition. In this paper, we propose a two-pathway graph-based model that involves the visual pathway to process visual data and the linguistic pathway to process linguistic data. In the visual pathway, we first extract the initial visual feature vectors of input images via pre-trained convolutional neural networks [1]. Then, we project the visual features to a latent space, obtaining the encoded visual features. Because directly applying the encoded features to recognize unseen compositions usually results in misclassification of similar compositions, we propose a composition clustering mechanism to cluster images belonging to the same composition. The composition clustering mechanism re-represents each image by measuring its similarity with all other images, and it outputs the compact visual features. In the linguistic pathway, to explore the interdependence between the attributes and objects, we propose an attribute-object semantic association graph network, which is implemented by the graph convolutional network (GCN) [22], [23], [24], [25], [26], [27]. Each node in the graph represents the linguistic feature (word embeddings) of an attribute or object entity, and the graph network outputs the encoded linguistic features in the latent space. The motivations for using a graph to encode linguistic information are two-fold: 1) The complex interdependence between the attributes and objects can be explicitly modeled via the graph, in which a large connection strength indicates an obvious semantic correlation between two nodes. 2) A graph is flexible and extensible while handling the multi-attribute-object composition recognition. With the computed compact visual features and the encoded linguistic features, the model is optimized by minimizing the Euclidean distance between two kinds of features.

We first evaluate our model on two commonly-used benchmark datasets, the MIT-States [28] and the UT-Zappos50K [29] dataset. On both datasets, our model achieves competitive recognition accuracies. Then, we move on to the Multi-Attribute Dataset (MAD). In this highly complex dataset with large variations in attribute and object distributions, our model outperforms the state-of-the-art baseline methods by large margins. In addition, by performing ablation experiments, it has been demonstrated that 1) a composition clustering mechanism contributes to learning compact representations, which allows the model to enlarge the margin between different compositions and distinguish the compositions that have similar appearances, and 2) the attribute-object semantic association graph in our model is expected to explore the semantic and contextual relations between the attributes and objects, which is significant for composition recognition.

In this work, we show that our model can learn concepts (i.e. attributes and objects) from seen compositions and transfer these learned concepts to recognize unseen compositions. We achieve this goal by designing an attribute-object semantic association graph-based model, which fuses visual and linguistic two-modal data. The main contributions of this paper can be summarized as follows.

- We introduce a novel yet simple composition clustering mechanism to compact intra-class image features, which reduces the misclassification of similar inter-class images.
- We build a semantic association graph over the attributes and objects and map the binary graph to a set of interdependent node representations to explore the inner relations between the attributes and objects.
- We built a multi-attribute dataset called MAD. To the best of our knowledge, MAD is the first dataset for inferring unseen multi-attribute-object compositions. We hope that MAD can promote the further development of related research in computer vision community.

2 RELATED WORK

2.1 Unseen Attribute-Object Composition Recognition

The intuitive idea to recognize unseen attribute-object compositions is combining attribute classifiers and object classifiers [12], [15]. However, these classifier-based methods separately process the attributes and objects, ignoring the interdependent relations between the attributes and objects. As a result, these methods do not achieve satisfied performance and suffer from the “domain shift” problem [30] - the distribution of the testing data is different from that of the training data. To explicitly factor out the attributes’ effect from their corresponding attribute-object composition representations, Nagarajan *et al.* [17] propose to model an attribute as an *operator* and an attribute-object composition as an object vector that is “operated” by the *operator*. However, such linear and explicit matrix transformation may be insufficient to represent various attribute concepts, and Li *et al.* [16] propose a symmetry principle to learn the coupled and decoupled representations of attributes and objects in the group theory framework. Recently, generative models

have been proved to be powerful in modeling data distributions. Nan *et al.* [20] introduce a generative model with the encoder-decoder mechanism to learn the intrinsic visual features and Wei *et al.* [21] propose to generate positive and (semi-) negative compositions to learn relations between the attributes and objects in an adversarial manner.

2.2 Zero-shot Learning

Zero-shot Learning (ZSL) aims to recognize unseen concepts (usually referring to objects) after learning only from training seen concepts and additional high-level semantic information (e.g. attributes and text). In the ZSL setting, the training label set and testing label set are disjoint. Early works [31], [32] typically extract visual feature in the visual space and project it into the semantic space where the attribute descriptions of unseen objects are known, and the recognition is implemented by searching the object whose description mostly matches the visual feature. For these methods, attribute classifiers are trained separately and the relations between attributes are ignored. In order to mitigate this issue, some works [33], [34] seek to embed the visual features and the attribute descriptions into a common latent space. However, the above methods lack either the ability to learn the bi-directional mappings between the visual space and the semantic/latent space or a flexible metric to evaluate the similarity between different kinds of features. Huang *et al.* [35] leverage generative adversarial networks (GAN) to generate various visual features conditioned on class labels and map each visual feature to its corresponding semantic feature. Apart from learning mappings between the visual space and semantic space, some useful techniques have been introduced in ZSL to improve recognition performance, such as memory mechanism [9], knowledge graph [36], [37] and low rank constraint [38]. A good survey of ZSL can be seen in [39].

2.3 Graph Convolutional Networks

Researchers have proposed to tackle object recognition problem via a graph to exploit complex relations between entities. Let $\mathcal{G} = (\mathcal{V}, \mathcal{A}, Z)$ denote a graph, where \mathcal{V} denotes the set of N nodes and \mathcal{A} is the adjacency matrix of the graph, which represents connection relation between edges. $Z \in \mathbb{R}^{N \times d}$ is a matrix that encodes node features, and Z_i describes the attribute feature associated with node i . To extend powerful convolutional neural network (CNN) to deal with graph-structured data, Bruna *et al.* [40] model convolutional operation in the Fourier domain by computing the eigen-decomposition of the graph Laplacian, resulting in a heavy computation burden. Kipf *et al.* [24] propose graph convolutional networks (GCN) to simplify the previous methods via a localized first-order approximation of spectral graph convolutions. Actually, the relations between objects are much complex in many applications. To encode high-order data correlation, Raman *et al.* [41] propose a hyper graph neural network by extending simple graph to hyper graph whose edge links more than two nodes. Recently, graph is used to deal with ZSL. Kato *et al.* [42] propose to compose classifiers for verb-noun pairs with GCN to recognize unseen human-object interactions. Wang *et al.* [36] use semantic embeddings of a category and knowledge

graph encoding the relation of a novel category to familiar categories to predict object classes.

3 METHODS

3.1 Problem Formulation

For unseen attribute-object composition recognition, the training set (seen compositions) is defined as $S = \{x_i^s, (a_i^s, o_i^s)\}_{i=1}^{n_s}$, where x_i^s is the i -th training image, and $(a_i^s, o_i^s) \in L^s$ is its corresponding attribute label and object label. The testing set (unseen compositions) is defined as $U = \{x_j^u, (a_j^u, o_j^u)\}_{j=1}^{n_u}$, where x_j^u is the j -th testing image, and $(a_j^u, o_j^u) \in L^u$ is its corresponding attribute label and object label. The seen composition set and unseen composition set are disjoint, i.e. $L^s \cap L^u = \emptyset$.

3.2 Method Overview

We propose a two-pathway model consisting of a visual pathway to process visual data and a linguistic pathway to process linguistic data. In the visual pathway, given a batch of images (batch-size = b), a pre-trained convolutional neural network is used to extract the m -dimensional initial visual features $X^0 \in \mathbb{R}^{b \times m}$, which is further processed by the visual encoder module and composition clustering mechanism, obtaining k -dimensional clustered visual features $X^c \in \mathbb{R}^{b \times k}$ in a latent space. In the linguistic pathway, all N attributes and object labels are embedded as $Z^0 \in \mathbb{R}^{N \times d}$ via a pre-trained linguistic model, which are used to initialize the attribute-object semantic association graph. Each node in the graph is a d -dimensional embedding feature representing an attribute or an object. After applying graph convolutional operations on Z^0 , we finally obtain the linguistic encoded feature matrix $Z \in \mathbb{R}^{N \times k}$ in the latent space.

During the training, we optimize the L2 loss between X^c and Z to fit the input images to the corresponding linguistic labels. During the testing, we identify the attribute-object composition label of a given image from all possible compositions by searching for the composition that has the nearest L2 distance to the clustered visual feature of the given image.

3.3 Network Architecture and Data Flow

3.3.1 Visual Encoder

Given a batch of b input images, we use a pre-trained convolutional neural network to extract m -dimensional image features, obtaining the initial image features $X^0 \in \mathbb{R}^{b \times m}$. Then, we use a visual encoder module $f_{en}(\cdot)$ to further process X^0 , which is implemented by fully connected layers with a linear activation function. The transformation is defined as follows:

$$X = f_{en}(X^0; \phi) \quad (1)$$

where ϕ represents the learnable parameters in the visual encoder $f_{en}(\cdot)$ and $X \in \mathbb{R}^{b \times k}$ represents the k -dimensional image features.

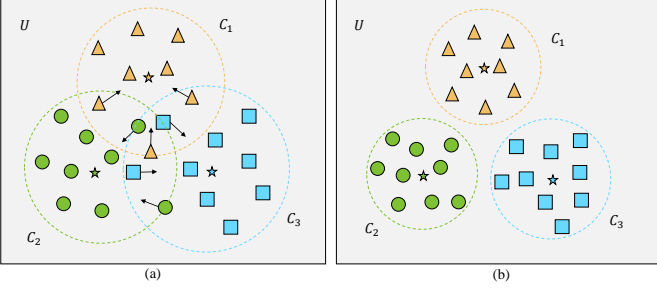


Fig. 1: A toy example illustrating the composition clustering mechanism. For simplicity, we assume that there are three classes C_1 , C_2 and C_3 . The circle indicates how large each corresponding class occupies in the full space U . (a) In practice, the three different circles will intersect with one another, which leads to misclassification. We hope to *pull* these points to the center of the corresponding category. (b) The ideal results after applying composition clustering.

3.3.2 Composition Clustering Mechanism

The highly semantic-related attributes (e.g. synonyms and near-synonyms) usually exhibit similar appearances, leading to the difficulty of distinguishing similar images that belong to different compositions. Therefore, we propose a simple composition clustering mechanism to solve the problem. Let us consider a toy example of ternary classification (Figure. 1). The full-space U contains n sample points (i.e. image features) belonging to three different types of compositions (i.e. C_1 , C_2 and C_3). The star denotes the centroid of the composition, and the circle indicates the boundary of each class. In practice, the samples within the intersecting area of different classes are easily misclassified. An intuitive idea to reduce the misclassification is to *pull* samples within the intersecting area to their correct cluster centroids (Figure. 1a). To accomplish this goal, we represent sample x_i via a weighted sum of all samples in the batch: $x_i = \sum_{j=1}^n w_j x_j$. The key point is to determine the weights w . Although an image could be similar to images belonging to other compositions, it will be more similar to images belonging to its own composition in most cases. Therefore, we can use the similarities between the samples as weights. Since we have recharacterized all of the samples, the centroid of each category will change accordingly, and the boundary tends to be smaller (Figure. 1b).

According to the above idea, given $X \in \mathbb{R}^{b \times k}$ as defined in Eq. 1, the composition clustering mechanism represents image i by the convex combination of these b image features:

$$X_i^c = \sum_{j=1}^b c_{ij} X_j \quad (2)$$

where c_{ij} is the combination coefficient that measures the similarity between X_i and X_j and satisfies $\sum_{j=1}^b c_{ij} = 1$, $c_{ij} \geq 0$. Here, we implement the convex combination of X in a self-representation way:

$$X^c = \text{softmax}(XX^T)X \quad (3)$$

where we use the inner product XX^T to measure the similarity between every two image features, and the

$\text{softmax}(\cdot)$ function normalizes the similarity matrix. Ideally, if the b images belong to the same category, then the features after this transformation will become more compact. Because objects of the same class have a similar appearance, then each coefficient in Eq. 2 will be large. Therefore, each feature has a large offset toward the center of these features. In the worst case, if the b images belong to b different categories, then each coefficient in Eq. 2 will be small, except for the coefficient obtained by the inner product of each image and itself, resulting in almost no movement of the image features. Therefore, after applying the composition clustering mechanism on X , the image features belonging to the same composition tend to be compact, and the image features corresponding to different compositions tend to be separated.

3.3.3 Visual Decoder

Inspired by the auto-encoder architecture, we design the visual decoder function $f_{de}(\cdot)$ to project X^c as \hat{X} to reconstruct the initial image feature X^0 :

$$\hat{X} = f_{de}(X^c; \theta) \quad (4)$$

where θ represents the learnable parameters in the decoder $f_{de}(\cdot)$, and \hat{X} is the reconstruction of the original visual features. The motivation for designing the visual decoder is to learn the intrinsic representation of X^c by minimizing the differences between \hat{X} and X^0 .

3.3.4 Linguistic Encoder

The relations of attribute-attribute, object-object and attribute-object are complex, such as folded box/unfolded box (antonym compositions) and traffic light/traffic sign (high co-occurrence objects). To encode these complex relations, we use the graph convolutional network (GCN) to propagate and aggregate information, in which the graph nodes represent attributes/objects. GCN is a multilayer neural network with a convolution operation defined on a graph. For the first layer, we initialize the graph feature matrix $Z^0 \in \mathbb{R}^{N \times d}$ by extracting the N attributes and object feature vectors with pre-trained word embedding models, where d is the dimensionality of the word embedding vectors. By default, we use the Glove [43] model to extract the linguistic features.

The next key is to determine the adjacency matrix $A \in \mathbb{R}^{N \times N}$. In this paper, we construct four different kinds of attribute-object semantic association graphs to explore a reasonable graph structure to model the relations between the attributes and objects. The four graphs are the vanilla random graph, sparse random graph, link graph and embedding graph. By randomly initializing the learnable adjacency matrix, we obtain the vanilla random graph (i.e. all nodes in the graph are randomly connected). What's more, not all attribute-object compositions are linguistically and physically meaningful in the real world, such as "flying dog" and "sliced boat". To disable unreasonable node connections, we regularize the randomly initialized adjacency matrix with the L1 norm constraint to make the graph sparse, obtaining the sparse random graph. For the link graph, two nodes can be linked if these two nodes correspond to an existing composition of the training set. For

example, the node representing “clean” is linked to the node “room” when “clean room” is in the training set. In terms of the embedding graph, since we encode attribute and object labels with word embeddings, it is natural to consider that two nodes are connected if the distance between their word embeddings is lower than a threshold. Motivated by this work [44], we compute $A(i, j)$ of the embedding graph by a Gaussian diffusion kernel:

$$A(i, j) = \exp \left(-\frac{\|Z_i^0 - Z_j^0\|_2^2}{\sigma^2} \right) \quad (5)$$

where Z_i^0 and Z_j^0 are the i -th and j -th rows of Z^0 , and σ is a hyper-parameter. However, due to the inaccurate semantic correlations caused by the introduction of the word embedding model, there could be some noisy connections. Thus, we binarize A in Eq. 5 to be a 0-1 matrix to filter out the noisy connections:

$$A = \mathcal{I}_{A(i, j) > t} \quad (6)$$

where \mathcal{I} is the indicator function, and t is a threshold value. In the experiment, we observe that the sparse random graph consistently performs better than other graphs. Therefore, we use the sparse random graph throughout the paper if not specified.

The following layer takes the previous layer feature matrix $Z^l \in \mathbb{R}^{N \times d_l}$ and the adjacency matrix A (where d_l indicates the dimensionality of node representations) as inputs, and it outputs the updated node representations $Z^{l+1} \in \mathbb{R}^{N \times d_{l+1}}$. Specifically, the propagation rule of the l -th layer is defined as:

$$Z^{l+1} = f(\hat{A}Z^lW^l) \quad (7)$$

where \hat{A} is the normalized adjacency matrix, W^l is layer-specific learnable parameters and $f(\cdot)$ represents an activation function, which is acted by the LeakyReLU [45] in our experiments. For the last layer, the output of the GCN is $Z \in \mathbb{R}^{N \times k}$, where k denotes the dimensionality of the common latent space.

3.4 Loss Functions

3.4.1 Fusion Loss

To fuse information in the visual pathway and linguistic pathway, we utilize the L2 loss to measure the difference between the clustered visual features X^c and the linguistic encoded feature Z :

$$L_{fus} = \|X^c - YZ\|_2 \quad (8)$$

Due to the shape mismatch between $X^c(b \times k)$ and $Z(N \times k)$, the Euclidean distance cannot be used directly. Thus, we design a mask matrix $Y(b \times N)$ to match the shapes of X^c and Z . In the single-attribute recognition, each row of Y contains two ones to index positions of the attribute and object labels of the corresponding image from the linguistic feature matrix Z , and the remaining elements are zeros. In multi-attribute recognition, each row of Y contains more than two ones to index positions of the attribute and object labels, and the remaining elements are zeros.

3.4.2 Triplet Loss

In view of the similar attribute-object composition recognition, the fusion loss is insufficient to discriminate similar compositions. Therefore, we introduce the standard triplet loss, which is formulated as:

$$L_{tri} = \max(0, d(X^c, YZ) - d(X^c, \tilde{Y}Z) + m) \quad (9)$$

where $d(\cdot, \cdot)$ denotes the Euclidean distance, m is the margin, and \tilde{Y} represents the negative mask matrix (different from the positive mask matrix Y). In fact, the triplet loss encourages the anchor X^c to be close to the positive sample YZ and away from the negative sample $\tilde{Y}Z$.

3.4.3 Decoding Loss

Inspired by recent work [20] on unseen attribute-object composition recognition, we introduce the decoding loss to minimize the L2 distance between the initial visual feature X^0 and the reconstruction visual feature \hat{X} :

$$L_{de} = \|X^0 - \hat{X}\|_2 \quad (10)$$

3.5 Learning and Inference

During the training, the goal is to learn the optimal parameters that minimize the overall loss:

$$L(W) = \alpha L_{fus} + \beta L_{tri} + \gamma L_{de} \quad (11)$$

where W represents all of the learnable parameters in the network. We use ADAM [46] as our optimizer.

During the inference, the clustered visual features X^c in a batch are computed. At the same time, we compute the linguistic encoded features Z , which are then multiplied by a mask matrix $Y^{test} \in \{0, 1\}^{N_u \times N}$ to obtain the linguistic features of all N_u possible attribute-object compositions. In the closed metric, N_u equals the number of unseen classes. In the open metric, N_u is the number of seen and unseen compositions. By computing the L2 distance between the clustered visual feature and the linguistic features of all possible compositions, the composition corresponding to the minimum L2 distance is taken as the attribute-object composition recognition result.

4 EXPERIMENTS

4.1 Datasets

We evaluate the proposed model on two public datasets, the MIT-States dataset [28] and the UT-Zappos50K dataset [29]. The MIT-States dataset is composed of 63,440 images, covering 115 attribute classes, 245 object classes, and 1,962 attribute-object compositions. Each image is annotated with an attribute-object composition label such as “clean kitchen”. The same settings are used as in previous works [15], [17], [20], [21]: 1,262 compositions/34,562 images are used for the training, and 700 compositions/19,191 images for the testing. UT-Zappos50K is a fine-grained shoes dataset with 50,025 images, including 16 attribute classes, 12 object classes, and 116 attribute-object compositions. Following the settings in previous works [15], [17], [20], [21], we use 83 compositions/24,898 images for the training and 33 compositions/4,228 images for the testing. The training and testing compositions are non-overlapping for both datasets.

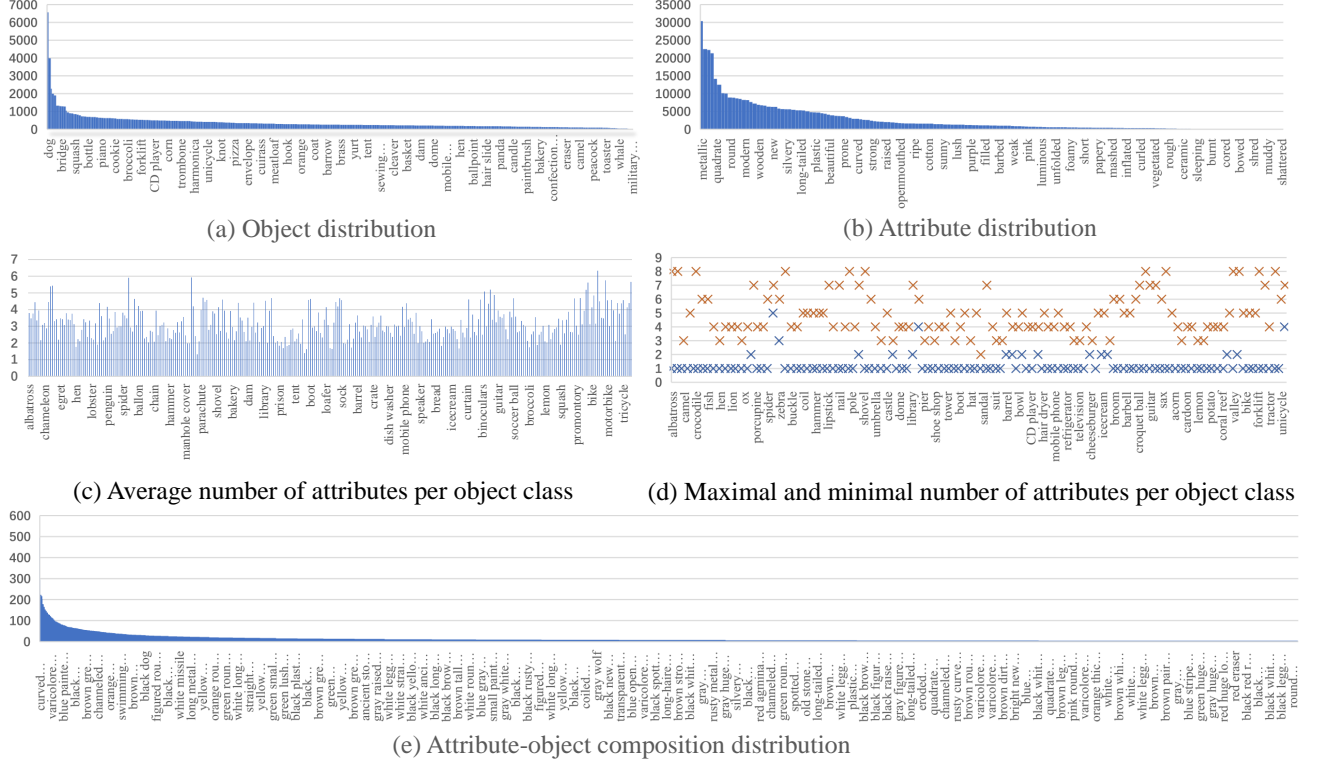


Fig. 2: Statistical distributions of the MAD dataset.

TABLE 1: Statistics of datasets.

Datasets	attribute classes	object classes	compositions	training compositions	testing compositions	images	training images	testing images	attribute per image
MIT-States	115	245	1,962	1,262	700	63,400	34,562	19,191	1
UT-Zappos50K	16	12	116	83	33	50,025	24,898	4,228	1
MAD	158	309	8,030	5,621+402	2,007	116,099	81,265+5,805	29,029	1-8

However, for both the MIT-States and UT-Zappos50K datasets, each image is annotated with a single attribute, which could be one-sided (i.e. causing ambiguity) and inaccurate for the co-occurrence patterns of the attributes. In addition, these two datasets suffer from data insufficiency (some compositions with less than 5 images). Therefore, we annotated a large-scale Multi-Attribute Dataset (MAD). Each image is annotated with one to eight salient attributes, considering different types of attribute categories (e.g. color, shape, motion, and texture). In total, 158 attributes and 309 objects are involved in the MAD dataset, and it covers more attributes and object categories than the MIT-States and UT-Zappos50K datasets. Figure. 2 shows some basic statistical distributions of the MAD dataset and Table. 1 summarizes the main differences between these three datasets.

4.2 Baselines and Metrics

Six baseline methods are compared with our method. We briefly introduce the baselines as follows:

- VISPRODNN [12] trains two independent classifiers to predict attributes and objects;
- SAE [19] projects the input feature into a semantic space where the auxiliary information of unseen pairs is known, and the recognition is then realized by finding the pair

whose auxiliary information is closest with the input feature;

- REDWINE [15] uses pre-trained linear SVM weights to replace the word vectors and trains a neural network to recognize unseen attribute-object compositions;

—ATTOPERATOR [17] is a state-of-the-art method that predicts unseen compositions by comparing the visual feature of the given image with all possible attribute-object features. The main idea is taking the attribute as the *operator* and the attribute-object composition is modeled as the object vectors transformed by the attribute *operator*;

- GENERATE [20] is a state-of-the-art method adopting the auto-encoder mechanism that reconstructs the input image features to recognize unseen compositions;

—ADVERSARIAL [21] is a state-of-the-art method adopting the adversarial learning to predict unseen compositions by comparing the distance between the generated semantic features of all candidate compositions from available word vectors with the visual feature of the given image.

We report the top-1 accuracy on the unseen testing set via three metrics, which are widely adopted by the state-of-the-art methods [17], [21]. 1) Closed: composition candidates to be tested are restricted to the unseen classes. The closed testing reduces the search space and usually achieves better performance. 2) Open: composition candidates to be tested

TABLE 2: Comparison results of the proposed model and the baseline methods on the MIT-States, UT-Zappos50K and MAD datasets (%). We widely compare our model with discriminative and generative models. For all of the baseline methods, we simply use the average value of the attribute features to adapt the multi-attribute situation on the MAD dataset.

Methods	MIT-States			UT-Zappos50K			MAD		
	closed	open	h-mean	closed	open	h-mean	closed	open	h-mean
Chance	0.14	0.05	0.07	3.0	0.9	1.4	0.05	0.01	0.02
VISPRODNN	13.9	2.8	4.7	49.9	4.8	8.8	12.1	0.32	0.62
SAE	13.7	3.4	5.4	26.9	3.2	5.8	17.3	5.3	8.1
REDWINE	12.5	3.1	5.0	40.3	2.1	4.0	0.4	0.07	0.12
OPERATOR	12.0	11.4	11.7	33.2	23.4	27.5	6.3	5.4	5.8
GENERATE	17.1	4.4	7.0	45.0	16.5	24.2	21.3	6.7	10.1
ADVERSARIAL	13.9	12.3	13.1	52.1	48.4	50.2	4.3	1.2	1.8
OUR	27.5	12.7	17.4	59.4	41.6	48.9	33.3	10.5	16.0

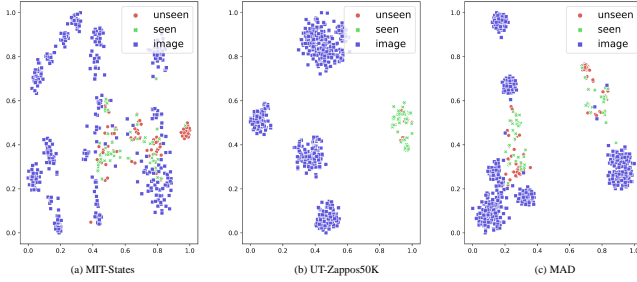


Fig. 3: We illustrate the challenge on the open metric by projecting the testing image features along with the testing label (unseen) and training label (seen) embeddings into a 2-dimensional space. Under the open metric, the testing image features may be closer to training labels (seen) than testing labels (unseen).

include both seen and unseen classes. As can be seen in Figure. 3, the testing image features may be closer to seen classes than unseen classes. Therefore, the open testing is more challenging. 3) H-mean: harmonic mean of the closed and open metrics to balance their performance, defined as $h - mean = 2 \times closed \times open / (closed + open)$.

4.3 Implementation Details

We use the ResNet-18 [1] network pre-trained on the ImageNet [47] dataset to extract the 512-dimensional initial visual features of the input images. For a fair comparison, neither a fine-tuning operation nor data augmentation is applied to our method and the baseline methods. We use the GloVe [43] model to extract the 300-dimensional linguistic attribute and object features. The visual pathway is composed of three fully-connected layers with the output dimensions of $1024 \rightarrow 2048 \rightarrow 1024$, and the linguistic pathway (i.e. GCN) is composed of three convolutional layers with the output channel numbers $1024 \rightarrow 2048 \rightarrow 1024$. In the comparative experiments on the MAD dataset, we simply use the average value of the attribute features to adapt the multi-attribute situation for all of the baseline methods, because they are originally designed to address single-attribute-object composition recognition. All of the experiments are performed on an Nvidia RTX 2080Ti GPU.

4.4 Single-Attribute-Object Composition Recognition

Table. 2 shows the comparison results of our method with baseline methods. On the MIT-States dataset, our method outperforms the baseline methods, achieving 60.8% (closed), 3.3% (open) and 32.8% (h-mean) improvements over the second-best methods. On the UT-Zappos50K dataset, our method behaves better than the ADVERSARIAL [21] method on the closed metric. However, on the open and h-mean metric, our method performs worse than the state-of-the-art. UT-Zappos50K is a fine-grained shoes dataset, thus the input node representations share similar semantic meanings. For our graph-based model, the representation of a node is iteratively computed by aggregating its neighboring node representations. As a result, the node representations are inclined to converge to a certain value as the message passes over the graph and thus become indistinguishable.

4.5 Multi-Attribute-Object Composition Recognition

On the MAD dataset, our method outperforms all of the baseline methods on all three metrics by large margins, achieving 56.3% (closed), 56.7% (open) and 58.4% (h-mean) improvements over the second-best method (Table. 2). Although ADVERSARIAL achieves the state-of-the-art performance on the single-attribute recognition, it gains relatively low performance under the multi-attribute recognition situation. The main reason is that the semi-negative compositions cannot be uniquely determined (i.e. ill-defined) on the MAD dataset, which confuses the network and leads to optimization difficulties. In contrast, our graph model can be flexibly extended from single-attribute to multi-attribute recognition.

4.6 Distinguishing Similar Attribute-Object Compositions

The goal of a composition clustering mechanism is to improve the ability of distinguishing similar attribute-object compositions. In this experiment, we study the effect of the composition clustering mechanism on the performance of our model. By designing ablation experiments, we test the recognition accuracies of two base models as well as base models after applying the composition clustering mechanism. The two base models are called the BASE-FC model and BASE-GCN model. The BASE-GCN model

TABLE 3: Ablation studies of the composition clustering mechanism on the MIT-States, UT-Zappos50K and MAD datasets (%). BASE-GCN and BASE-FC are two base models. BASE-GCN represents removing the composition clustering mechanism on the proposed model. BASE-FC denotes removing the composition clustering operation and substituting the GCN with an equal number of fully connected layers (FC). Then, we obtain the BASE-GCN+CC and BASE-FC+CC models by applying the composition clustering (CC) operation on the base models.

Ablation tests	MIT-States			UT-Zappos50K			MAD		
	closed	open	h-mean	closed	open	h-mean	closed	open	h-mean
BASE-GCN	16.4	4.7	7.3	38.5	16.2	22.8	28.4	8.5	13.1
BASE-GCN+CC	27.5	12.7	17.4	59.4	41.6	48.9	33.3	10.5	16.0
BASE-FC	17.1	5.3	8.1	40.4	16.2	23.1	23.1	7.4	11.2
BASE-FC+CC	26.5	11.6	16.1	55.8	26.2	35.7	26.0	8.3	12.6

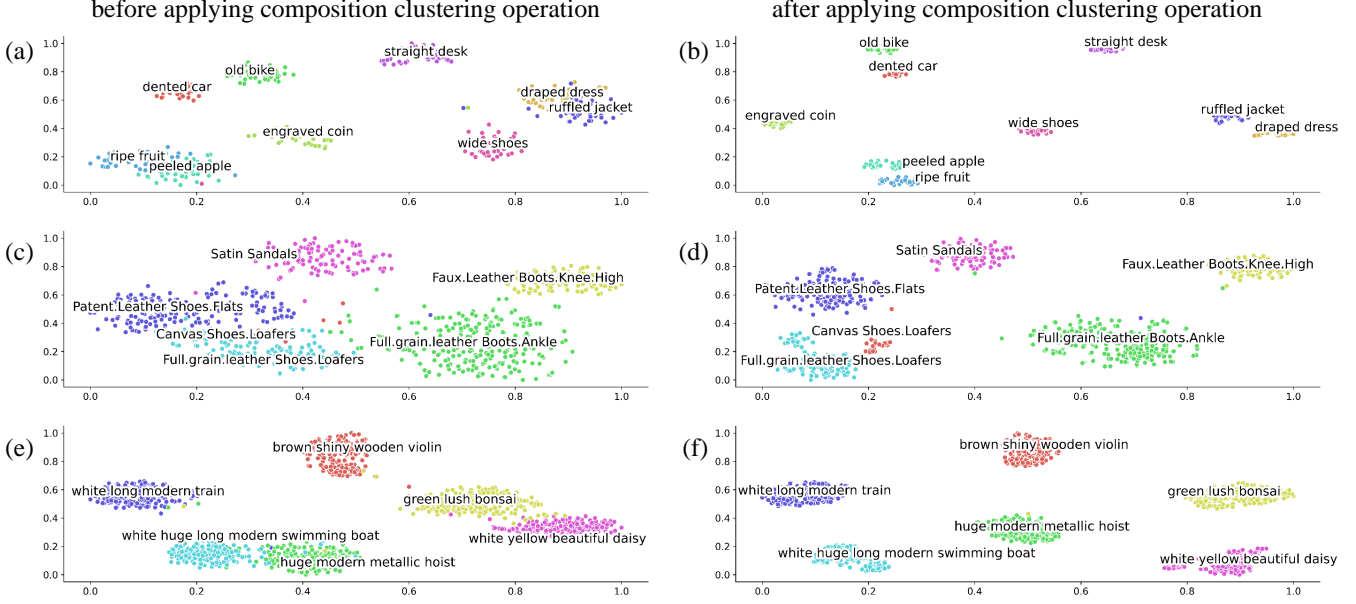


Fig. 4: Effects of the composition clustering mechanism. We demonstrate the effectiveness of the composition clustering mechanism by comparing the distribution of the image features obtained before applying composition clustering and after applying composition clustering. Hundreds of image features extracted before applying composition clustering are projected to a 2-dimensional space with the t-SNE algorithm on the MIT-States (a), UT-Zappos50K (c) and MAD (e) datasets. Meanwhile, hundreds of image features extracted after applying composition clustering are projected to a 2-dimensional space with the t-SNE algorithm on the MIT-States (b), UT-Zappos50K (d) and MAD (f) datasets. For convenience of comparison, we normalize the features to the interval of $[0, 1]$. Different colors indicate different compositions, and the text over each cluster is its composition label. As can be seen, the image features of the same composition become compact and the margins between different compositions are enlarged after applying the composition clustering operation.

represents removing the composition clustering mechanism. The BASE-FC model denotes removing the composition clustering operation and substituting the GCN with an equal number of fully connected layers (FC). Then, we obtain the BASE-GCN+CC and BASE-FC+CC models by applying the composition clustering (CC) operation on the base models.

As shown in Table. 3, for both the BASE-GCN and BASE-FC models, using the composition clustering mechanism contributes to consistent and considerable improvements on all three datasets over three metrics, which demonstrates the significance of the composition clustering mechanism. The composition clustering mechanism aims to cluster similar data points in the latent space, which benefits improving the separability of different compositions. Therefore, it boosts the performance of distinguishing compositions with simi-

lar appearances.

To test the significance of the composition clustering mechanism qualitatively, we visualize the encoded image features X (before applying the composition clustering operation) and the compact image features X^c (after applying the composition clustering operation) using the t-SNE [48] algorithm. As shown in Figure. 4b (MIT-States dataset), Figure. 4d (UT-Zappos50K dataset) and Figure. 4f (MAD dataset), we observe that the samples of the same composition become compact and the margin between different compositions is enlarged after applying the composition clustering mechanism. Meanwhile, semantically related compositions are close to one another. For example, “ruffled jacket” and “draped dress”, belonging to the same super-class of clothes, are located closely to each other (lower right of Figure. 4b), and “old bike”, “dented car”, belonging

TABLE 4: Effects of different graph construction methods on the MIT-States, UT-Zappos50K and MAD datasets (%). Vanilla random represents randomly initializing the graph. Sparse random denotes adding sparse constraints on the basis of the random graph. The link graph is constructed by connecting nodes if the corresponding composition is in the training set. The embedding graph is constructed by measuring the distances between the attributes and objects linguistic features.

Graphs	MIT-States			UT-Zappos50K			MAD		
	closed	open	h-mean	closed	open	h-mean	closed	open	h-mean
Vanilla random	27.1	12.5	17.1	58.4	40.5	47.8	31.7	10.0	15.2
Sparse random	27.5	12.7	17.4	59.4	41.6	48.9	33.3	10.5	16.0
Link	22.5	9.5	13.4	35.6	21.3	26.7	22.4	5.4	8.7
Embedding	27.5	12.5	17.2	57.5	36.3	44.5	31.4	9.7	14.8
Non-graph	26.5	11.6	16.1	55.8	26.2	35.7	26.0	8.3	12.6

TABLE 5: Comparison results of the proposed model with different network architectures of feature extractors on the MIT-States, UT-Zappos50K and MAD datasets (%). We compare the performance of different visual feature extractors and linguistic feature extractors.

Feature extractors	Network architectures	MIT-States			UT-Zappos50K			MAD		
		closed	open	h-mean	closed	open	h-mean	closed	open	h-mean
Visual feature extractors	VGG-16	14.4	5.0	7.4	36.8	18.3	24.4	21.7	6.5	10.0
	VGG-19	15.0	5.0	7.5	38.0	18.4	24.8	22.7	6.9	10.6
	ResNet-18	27.5	12.7	17.4	59.4	41.6	48.9	33.3	10.5	16.0
	ResNet-50	30.7	15.1	20.2	59.3	41.2	48.6	34.7	10.9	16.6
	ResNet-101	31.6	15.2	20.5	60.1	43.0	50.1	35.8	11.1	16.9
	GoogleNet	25.3	11.4	15.7	42.1	29.2	34.5	26.6	8.2	12.5
Linguistic feature extractors	Glove	27.5	12.7	17.4	59.4	41.6	48.9	33.3	10.5	16.0
	Word2Vector	28.1	12.7	17.5	59.9	38.5	46.9	31.3	9.9	15.0
	fastText	27.8	12.7	17.4	58.2	38.5	46.3	31.3	9.7	14.8
	One-hot	27.6	12.4	17.1	59.9	37.7	46.3	31.4	9.7	14.8

to the same super-class of transportation vehicle, are close to one another (top left of Figure. 4b). Comparatively, if a composition clustering mechanism is not applied, the samples are mixed together (Figure. 4a, c, e).

4.7 Modeling Attribute and Object Relations

In this experiment, we aim to explore a reasonable graph structure to model the relations between the attributes and objects. To compare with the four graph-based models (as defined in Section 3.3.4), we introduce a non-graph model by replacing the GCN with an equal number of fully-connected layers on the proposed model. As shown in Table. 4, the model with different graphs basically achieves satisfactory accuracies. After constraining the random graph with the L1 norm, we observe that the sparse random graph achieves slightly better performance than that of the vanilla random graph, proving that the sparse connection between the attributes and object nodes is beneficial to learn good node representations. In addition, we observe that the link graph achieves the lowest performance among all of the graph methods on these three datasets, which is due to the introduction of noisy connections in the graph. Importantly, compared with the other graph-based models except the link graph, the recognition performance of the non-graph model is reduced. Summarizing the above, a sparsely connected attribute-object semantic association graph contributes to learning good node representations and modeling meaningful relations, but a dense graph could introduce noisy connections.

4.8 Visual and Linguistic Feature Extraction

In Table. 5, we report the accuracies corresponding to different types of image feature extractors and word embeddings. Firstly, we test three kinds of image feature extractors, VGG [49], ResNet [1] and GoogleNet [50]. As can be seen, visual features significantly affect the recognition performance. Due to the residual connection [1], ResNet models usually behave better than VGG and GoogleNet, and they achieve higher accuracies with deeper architectures. Then, we study three widely used word embeddings including Glove [43], Word2Vector [51] and fastText [52] to investigate the effects of different word embeddings. As shown in Table. 5, the Glove method achieves competitive performance on all three datasets. In addition to the word embedding models, we also use the one-hot encoding of labels as the inputs of the linguistic pathway. As a simple method, the one-hot encoding scheme behaves worse than those methods that employ word embeddings. The main reason is that the one-hot encoding does not consider the semantic relations between different labels.

4.9 Image retrieval

To qualitatively evaluate the attribute-object interdependent relations that our model has learned, we report the image retrieval results from a given attribute-object composition query. For each dataset, we use the trained model to retrieve the top-5 nearest images to the given query from the testing set. In practice, a query, which arises from various compositions, is unknown in advance. To better evaluate image retrieval results under different situations,



Fig. 5: Image retrieval results. We show the image retrieval results under three different types of queries, i.e. unseen (in red box), seen (in purple box) and new (in blue box). (a)-(c) The top-5 nearest images to the given query from the testing set are shown for the MIT-States, UT-Zappos50K and MAD datasets, respectively. The text below shows the corresponding queries.

the queries are categorized into three types. 1) Unseen: queries are chosen from the testing label set. 2) Seen: queries are selected from the training label set. 3) New: queries are synthesized manually by arbitrarily choosing attributes and objects and composing them to ensure that the manipulated compositions are neither in the training label set nor in the testing label set. Compared with the first two cases, there is no corresponding image in the testing set, and the query has not been seen. Therefore, it is very challenging for a model to retrieve reasonable images. Meanwhile, this experiment can test whether a model has essentially learned the concepts.

Image retrieval results are shown in Figure. 5, where the first two columns represent the unseen queries, the middle two columns are seen queries, and the last two columns depict new queries. All of the queries are listed in the box below the images, in order. Our proposed model is capable of retrieving a certain number of accurate images on the MIT-States (Figure. 5a) and UT-Zappos50K (Figure. 5b) datasets. The task on the MAD dataset is more difficult than that on the other two datasets because each query is composed of multiple attributes, which requires a deeper understanding of the attributes and object concepts and the relations between them. Admittedly, the results on this complex dataset (Figure. 5c) suggest that our model has learned the concrete concepts and interdependent relations between the attributes and objects.

4.10 Ablation Studies for Loss Functions

In this experiment, we evaluate the effects of different loss compositions, and the results are shown in Table. 6. The fusion loss L_{fus} is taken as the basic loss, which fuses the visual and linguistic modal data. If it is only the basic loss that is used, the accuracies are relatively low on these three datasets. When the triplet loss L_{tri} is added to the basic loss (+tri), the accuracies slightly improve, validating the

effectiveness of the triplet loss. When the decoding loss L_{de} is added to the basic loss (+de), the model achieves a striking accuracy improvements on these three datasets, demonstrating that the decoding loss in the model is effective. It is also observed that the model obtains the highest accuracies when all losses are used (+tri+de), which further confirms the effectiveness of the losses.

4.11 Hyper-parameter Sensitivity

4.11.1 Batch-size

Since the composition clustering mechanism is related to the batch-size b in Eq. 3, which may have an influence on the recognition results, experiments are designed to test the performance of the composition clustering mechanism with different batch sizes. As is shown in Figure. 6, a more proper batch-size will contribute to better performance. A possible explanation for this phenomenon could be that too few samples in a batch are not sufficient to enable the learning of the relationships between samples, whereas too many samples in a batch increase the difficulty of clustering compositions due to the reason that more compositions are involved.

4.11.2 Different number of layers

Besides, the robustness of the model to the number of layers is examined in Table. 7. The 2-layer model has the output dimensions as $1024 \rightarrow 2048$ and the 4-layer model has the output dimensions as $1024 \rightarrow 2048 \rightarrow 1024 \rightarrow 1024$. Except for the shallow 1-layer model (output dimension being 1024), the recognition accuracies are robust to the depth of the model. The recognition accuracies raise as the depth of model increases from one layer to three layers, which is because a deeper model involves more convolution operations over the graph, a quality essential to aggregate information about distant nodes. Nevertheless, the performance drops

TABLE 6: The top-1 accuracies of different loss function compositions on the MIT-States, UT-Zappos50K and MAD datasets. Here, “fus”, “tri” and “de” represent the fusion loss L_{fus} , triplet loss L_{tri} and decoding loss L_{de} , respectively.

Loss	MIT-States			UT-Zappos50K			MAD		
	closed	open	h-mean	closed	open	h-mean	closed	open	h-mean
fus	7.7	2.6	3.9	10.3	5.4	7.1	8.0	1.6	2.7
+tri	9.1	3.1	4.6	15.0	6.5	9.1	7.7	2.0	3.2
+de	27.1	12.1	16.7	55.7	33.8	42.1	31.4	9.9	15.1
+tri+de	27.5	12.7	17.4	59.4	41.6	48.9	33.3	10.5	16.0

TABLE 7: Effects of different number of layers (%).

Layer	MIT-States			UT-Zappos50K			MAD		
	closed	open	h-mean	closed	open	h-mean	closed	open	h-mean
1	25.8	10.9	15.3	58.2	38.1	46.1	31.0	9.5	14.5
2	26.6	11.5	16.1	57.7	38.9	46.5	31.1	9.7	14.8
3	27.5	12.7	17.4	59.4	41.6	48.9	33.3	10.5	16.0
4	27.4	12.7	17.4	59.6	38.5	46.8	31.4	9.6	14.7

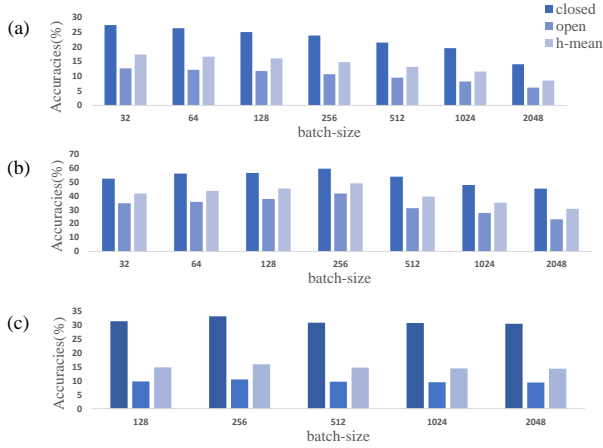


Fig. 6: Effects of batch-size b . (a) The top-1 accuracies on the MIT-States dataset. (b) The top-1 accuracies on the UT-Zappos50K dataset. (c) The top-1 accuracies on the MAD dataset.

slightly when the depths of a model increases to a certain point, possibly due to the over smoothing [53], [54] problem of GCN.

4.12 Graph Structure

After applying the sparse constraint to the adjacency matrix, the matrix is expected to be sparse (Figure. 7). For the clarity of visualization, certain rows and columns of the whole adjacency matrix are randomly selected. An obvious correlation between “cluttered” and “rope” is shown in Figure. 7a, yet there are no images labeled with “cluttered rope” in the MIT-States dataset. It is the model itself that infers some meaningful compositions, even if they do not appear in the dataset. Besides, the model trained on MAD also identifies a relationship between objects that are usually paired up in daily, e.g. “fountain pen” and “ballpoint” in Figure. 7c.

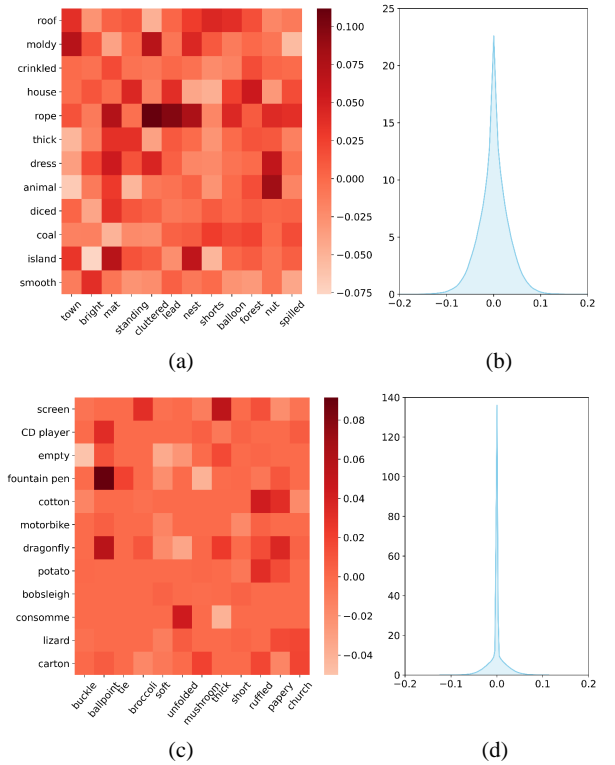


Fig. 7: Graph structure. We show the structure of the learned graph (i.e. the adjacency matrix) to illustrate some learned correlations. (a) The heatmap of randomly chosen columns and rows from the adjacency matrix learned on the MIT-States dataset, and (b) the density distribution curve of the adjacency matrix. (c) The heatmap of randomly chosen columns and rows from the adjacency matrix learned on the MAD dataset, and (d) the density distribution curve of the adjacency matrix.

5 CONCLUSION AND FUTURE WORK

This paper studies a problem called unseen attribute-object composition recognition. In view of the fact that images belonging to similar compositions usually lead to misclassification, we propose a novel composition clustering mechanism to distinguish similar compositions. Meanwhile, the attributes and objects are interdependent, and the relations between them are captured via a graph. The proposed model presents competitive performance and shows good flexibility and extensibility to handle the more challenging multi-attribute-object recognition problem. The t-SNE visualization results (Figure. 4) show that the composition clustering mechanism effectively compacts image features belonging to the same composition, enlarges the margin between different compositions and maintains a meaningful semantic topology. More qualitative results (Figure. 5, 7) illustrate that our model can learn the concepts of the attributes and objects and capture the complex correlations between them.

However, current progress is still far from human-like intelligence. From the perspective of attribute learning, there are at least two worthy research issues. 1) Elimination of attribute uncertainty: the attribute annotation task is subjective, and it could be difficult to determine whether an object contains an attribute or not. Thus, a practical way to eliminate this uncertainty (i.e. label ambiguity [55], [56]) is to quantify the degree to which an object has a certain attribute, i.e. the confidence in the attribute. 2) Multi-Attribute Multi-Object Composition (MAMOC) recognition: the real world usually involves multiple objects and each object has multiple attributes. Therefore, a good MAMOC recognition model will pave the way for high-level AI.

ACKNOWLEDGMENTS

This work is supported by the National Science Foundation of China (No. 61773312, 61790562, 61790563).

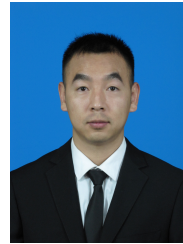
REFERENCES

- [1] K. He, X. Zhang, S. Ren, and J. Sun, "Deep residual learning for image recognition," in *IEEE Conference on Computer Vision and Pattern Recognition (CVPR)*, 2016, pp. 770–778.
- [2] D. Silver, A. Huang, C. J. Maddison, A. Guez, L. Sifre, G. V. Den Driessche, J. Schrittwieser, I. Antonoglou, V. Panneershelvam, M. Lanctot et al., "Mastering the game of go with deep neural networks and tree search," *Nature*, vol. 529, no. 7587, pp. 484–489, 2016.
- [3] D. Silver, J. Schrittwieser, K. Simonyan, I. Antonoglou, A. Huang, A. Guez, T. Hubert, L. Baker, M. Lai, A. Bolton et al., "Mastering the game of go without human knowledge," *Nature*, vol. 550, no. 7676, pp. 354–359, 2017.
- [4] Y. Lecun, Y. Bengio, and G. E. Hinton, "Deep learning," *Nature*, vol. 521, no. 7553, pp. 436–444, 2015.
- [5] R. L. Solso, M. K. MacLin, and O. H. MacLin, *Cognitive psychology (7th ed.)*. Pearson Education New Zealand, 2005.
- [6] J. Johnson, R. Krishna, M. Stark, L. Li, D. A. Shamma, M. S. Bernstein, and L. Feifei, "Image retrieval using scene graphs," in *IEEE Conference on Computer Vision and Pattern Recognition (CVPR)*, 2015, pp. 3668–3678.
- [7] Y. Lin, L. Zheng, Z. Zheng, Y. Wu, Z. Hu, C. Yan, and Y. Yang, "Improving person re-identification by attribute and identity learning," *Pattern Recognition*, vol. 95, pp. 151–161, 2019.
- [8] D. Xu, Y. Zhu, C. B. Choy, and L. Feifei, "Scene graph generation by iterative message passing," in *IEEE Conference on Computer Vision and Pattern Recognition (CVPR)*, 2017, pp. 3097–3106.
- [9] A. Santoro, D. Raposo, D. G. T. Barrett, M. Malinowski, R. Pascanu, P. W. Battaglia, and T. Lillicrap, "A simple neural network module for relational reasoning," in *Conference on Neural Information Processing Systems (NeurIPS)*, 2017, pp. 4967–4976.
- [10] B. J. Devereux, A. Clarke, and L. K. Tyler, "Integrated deep visual and semantic attractor neural networks predict fmri pattern information along the ventral object processing pathway," *Scientific Reports*, vol. 8, no. 1, p. 10636, 2018.
- [11] B. M. Lake, R. Salakhutdinov, and J. B. Tenenbaum, "Human-level concept learning through probabilistic program induction," *Science*, vol. 350, no. 6266, pp. 1332–1338, 2015.
- [12] C. Chen and K. Grauman, "Inferring analogous attributes," in *IEEE Conference on Computer Vision and Pattern Recognition (CVPR)*, 2014, pp. 200–207.
- [13] M. Elhoseiny, B. Saleh, and A. Elgammal, "Write a classifier: Zero-shot learning using purely textual descriptions," in *IEEE International Conference on Computer Vision (ICCV)*, 2013, pp. 2584–2591.
- [14] C. Lu, R. Krishna, M. S. Bernstein, and L. Feifei, "Visual relationship detection with language priors," in *European Conference on Computer Vision (ECCV)*, 2016, pp. 852–869.
- [15] I. Misra, A. Gupta, and M. Hebert, "From red wine to red tomato: Composition with context," in *IEEE Conference on Computer Vision and Pattern Recognition (CVPR)*, 2017, pp. 1160–1169.
- [16] Y.-L. Li, Y. Xu, X. Mao, and C. Lu, "Symmetry and group in attribute-object compositions," in *IEEE Conference on Computer Vision and Pattern Recognition (CVPR)*, 2020, pp. 11 316–11 325.
- [17] T. Nagarajan and K. Grauman, "Attributes as operators: Factorizing unseen attribute-object compositions," in *European Conference on Computer Vision (ECCV)*, 2018, pp. 172–190.
- [18] S. Purushwalkam, M. Nickel, A. Gupta, and M. Ranzato, "Task-driven modular networks for zero-shot compositional learning," in *IEEE International Conference on Computer Vision (ICCV)*, 2019, pp. 3593–3602.
- [19] E. Kodirov, T. Xiang, and S. Gong, "Semantic autoencoder for zero-shot learning," in *IEEE Conference on Computer Vision and Pattern Recognition (CVPR)*, 2017, pp. 4447–4456.
- [20] Z. Nan, Y. Liu, N. Zheng, and S.-C. Zhu, "Recognizing unseen attribute-object pair with generative model," in *The National Conference on Artificial Intelligence (AAAI)*, vol. 33, 2019, pp. 8811–8818.
- [21] K. Wei, M. Yang, H. Wang, C. Deng, and X. Liu, "Adversarial finegrained composition learning for unseen attribute-object recognition," in *IEEE International Conference on Computer Vision (ICCV)*, 2019, pp. 3741–3749.
- [22] Z. Chen, X. Wei, P. Wang, and Y. Guo, "Multi-label image recognition with graph convolutional networks," in *IEEE Conference on Computer Vision and Pattern Recognition (CVPR)*, 2019, pp. 5177–5186.
- [23] H. Gao and S. Ji, "Graph u-nets," *arXiv preprint arXiv:1905.05178*, 2019.
- [24] T. N. Kipf and M. Welling, "Semi-supervised classification with graph convolutional networks," *arXiv preprint arXiv:1609.02907*, 2016.
- [25] Y. Liu, X. Wang, S. Wu, and Z. Xiao, "Independence promoted graph disentangled networks," in *The National Conference on Artificial Intelligence (AAAI)*, 2020, pp. 4916–4923.
- [26] S. Vashishth, S. Sanyal, V. Nitin, and P. Talukdar, "Composition-based multi-relational graph convolutional networks," *arXiv preprint arXiv:1911.03082*, 2019.
- [27] P. Veličković, G. Cucurull, A. Casanova, A. Romero, P. Lio and Y. Bengio, "Graph attention networks," *arXiv preprint arXiv:1710.10903*, 2017.
- [28] P. Isola, J. J. Lim, and E. H. Adelson, "Discovering states and transformations in image collections," in *IEEE Conference on Computer Vision and Pattern Recognition (CVPR)*, 2015, pp. 1383–1391.
- [29] A. Yu and K. Grauman, "Fine-grained visual comparisons with local learning," in *IEEE Conference on Computer Vision and Pattern Recognition (CVPR)*, 2014, pp. 192–199.
- [30] Y. Fu, T. M. Hospedales, T. Xiang, and S. Gong, "Transductive multi-view zero-shot learning," *IEEE Transactions on Pattern Analysis and Machine Intelligence*, vol. 37, no. 11, pp. 2332–2345, 2015.
- [31] C. H. Lampert, H. Nickisch, and S. Harmeling, "Learning to detect unseen object classes by between-class attribute transfer," in *IEEE Conference on Computer Vision and Pattern Recognition (CVPR)*, 2009, pp. 951–958.
- [32] C. H. Lampert, H. Nickisch, and S. Harmeling, "Attribute-based classification for zero-shot visual object categorization," *IEEE*

- Transactions on Pattern Analysis and Machine Intelligence*, vol. 36, no. 3, pp. 453–465, 2014.
- [33] Y. Li, J. Zhang, J. Zhang, and K. Huang, “Discriminative learning of latent features for zero-shot recognition,” in *IEEE Conference on Computer Vision and Pattern Recognition (CVPR)*, 2018, pp. 7463–7471.
- [34] X. Wang, S. Pang, J. Zhu, Z. Li, Z. Tian, and Y. Li, “Visual space optimization for zero-shot learning,” *arXiv preprint arXiv:1907.00330*, 2019.
- [35] H. Huang, C. Wang, P. S. Yu, and C.-D. Wang, “Generative dual adversarial network for generalized zero-shot learning,” in *IEEE Conference on Computer Vision and Pattern Recognition (CVPR)*, 2019, pp. 801–810.
- [36] X. Wang, Y. Ye, and A. Gupta, “Zero-shot recognition via semantic embeddings and knowledge graphs,” in *IEEE Conference on Computer Vision and Pattern Recognition (CVPR)*, 2018, pp. 6857–6866.
- [37] M. Kampffmeyer, Y. Chen, X. Liang, H. Wang, Y. Zhang, and E. P. Xing, “Rethinking knowledge graph propagation for zeroshot learning,” in *IEEE Conference on Computer Vision and Pattern Recognition (CVPR)*, 2019, pp. 11 487–11 496.
- [38] Y. Liu, Q. Gao, J. Li, J. Han, and L. Shao, “Zero shot learning via low-rank embedded semantic autoencoder,” in *International Joint Conference on Artificial Intelligence (IJCAI)*, 2018, pp. 2490–2496.
- [39] Y. Xian, C. H. Lampert, B. Schiele, and Z. Akata, “Zero-shot learning—a comprehensive evaluation of the good, the bad and the ugly,” *IEEE Transactions on Pattern Analysis and Machine Intelligence*, vol. 41, no. 9, pp. 2251–2265, 2019.
- [40] J. Bruna, W. Zaremba, A. Szlam, and Y. LeCun, “Spectral networks and locally connected networks on graphs,” *arXiv preprint arXiv:1312.6203*, 2013.
- [41] M. G. Raman, N. Somu, K. Kirthivasan, and V. S. Sriram, “A hyper-graph and arithmetic residue-based probabilistic neural network for classification in intrusion detection systems,” *Neural Networks*, vol. 92, pp. 89–97, 2017.
- [42] K. Kato, Y. Li, and A. Gupta, “Compositional learning for human object interaction,” in *European Conference on Computer Vision (ECCV)*, 2018, pp. 234–251.
- [43] J. Pennington, R. Socher, and C. D. Manning, “Glove: Global vectors for word representation,” in *Conference on Empirical Methods in Natural Language Processing (EMNLP)*, 2014, pp. 1532–1543.
- [44] M. Henaff, J. Bruna, and Y. LeCun, “Deep convolutional networks on graph-structured data,” *arXiv preprint arXiv:1506.05163*, 2015.
- [45] A. L. Maas, A. Y. Hannun, and A. Y. Ng, “Rectifier nonlinearities improve neural network acoustic models,” in *IEEE International Conference on Machine Learning (ICML)*, 2013.
- [46] D. P. Kingma and J. Ba, “Adam: A method for stochastic optimization,” *arXiv preprint arXiv:1412.6980*, 2014.
- [47] J. Deng, W. Dong, R. Socher, L.-J. Li, K. Li, and L. Fei-Fei, “Imagenet: A large-scale hierarchical image database,” in *IEEE Conference on Computer Vision and Pattern Recognition (CVPR)*, 2009, pp. 248–255.
- [48] L. v. d. Maaten and G. E. Hinton, “Visualizing data using t-sne,” *Journal of Machine Learning Research*, vol. 9, no. Nov, pp. 2579–2605, 2008.
- [49] K. Simonyan and A. Zisserman, “Very deep convolutional networks for large-scale image recognition,” *arXiv preprint arXiv:1409.1556*, 2014.
- [50] C. Szegedy, W. Liu, Y. Jia, P. Sermanet, S. Reed, D. Anguelov, D. Erhan, V. Vanhoucke, and A. Rabinovich, “Going deeper with convolutions,” in *IEEE Conference on Computer Vision and Pattern Recognition (CVPR)*, 2015, pp. 1–9.
- [51] T. Mikolov, K. Chen, G. Corrado, and J. Dean, “Efficient estimation of word representations in vector space,” *arXiv preprint arXiv:1301.3781*, 2013.
- [52] A. Joulin, E. Grave, P. Bojanowski, M. Douze, H. Jegou, and T. Mikolov, “Fasttext.zip: Compressing text classification models,” *arXiv preprint arXiv:1612.03651*, 2016.
- [53] Q. Li, Z. Han, and X.-M. Wu, “Deeper insights into graph convolutional networks for semi-supervised learning,” *arXiv preprint arXiv:1801.07606*, 2018.
- [54] M. Chen, Z. Wei, Z. Huang, B. Ding, and Y. Li, “Simple and deep graph convolutional networks,” *arXiv preprint arXiv:2007.02133*, 2020.
- [55] B. Gao, C. Xing, C. Xie, J. Wu, and X. Geng, “Deep label distribution learning with label ambiguity,” *IEEE Transactions on Image Processing*, vol. 26, no. 6, pp. 2825–2838, 2017.
- [56] D. Tanaka, D. Ikami, T. Yamasaki, and K. Aizawa, “Joint optimization framework for learning with noisy labels,” in *IEEE Conference on Computer Vision and Pattern Recognition (CVPR)*, 2018, pp. 5552–5560.



Hui Chen received the B.Sc. degree from Xi'an Jiaotong University, Xi'an, China, in 2019, where he is currently pursuing the Ph.D. degree. His current research interests include zero-shot learning, attribute recognition, graph neural networks and self-supervised learning methods.



Zhixiong Nan is currently an assistant professor at Xi'an Jiaotong University. He received the Ph.D. degrees from Xi'an Jiaotong University in 2019. He was a joint Ph.D. student at the University of California, Los Angeles (UCLA) from 2017 to 2019. His research interests include human attention estimation and traffic scene understanding.



Jingjing Jiang received the B.S. degree in mechanical engineering from Xi'an Jiaotong University in 2017. She is currently a Ph.D. student with the Institute of Artificial Intelligence and Robotics of Xi'an Jiaotong University. Her research interests include computer vision and deep learning.



Nanning Zheng (SM'93, F'06) is a distinguished professor in the Institute of Artificial Intelligence and Robotics at Xi'an Jiaotong University. He graduated from the Department of Electrical Engineering, Xi'an Jiaotong University, Xi'an, China, in 1975, and received the M.S. degree in information and control engineering from Xi'an Jiaotong University in 1981 and the Ph.D. degree in electrical engineering from Keio University, Yokohama, Japan, in 1985. He is the founder of the Institute of Artificial Intelligence and Robotics at Xi'an Jiaotong University. He is currently a professor and director of the Institute of Artificial Intelligence and Robotics, Xi'an Jiaotong University. His research interests include computer vision, pattern recognition, autonomous vehicle and brain-inspired computing. Prof. Zheng became a member of the Chinese Academy of Engineering in 1999, and he is a Council Member of the International Association for Pattern Recognition (IAPR). Dr. Zheng is an IEEE Fellow and currently he is president of Chinese Association of Automation(CAA), vice president of Chinese Society for Cognitive Science (CSCS).